

Quench dynamics of a correlated quantum dot sandwiched between normal-metal and superconducting leads

K. Wrześniewski^{1,*}, B. Baran², R. Taranko², T. Domański^{2,†} and I. Weymann^{1,‡}

¹*Institute of Spintronics and Quantum Information, Faculty of Physics, Adam Mickiewicz University, 61-614 Poznań, Poland*

²*Institute of Physics, Maria Curie-Skłodowska University, 20-031 Lublin, Poland*



(Received 27 July 2020; revised 13 January 2021; accepted 12 April 2021; published 22 April 2021)

Quantum system abruptly driven from its stationary phase can reveal nontrivial dynamics upon approaching a new final state. We investigate here such dynamics for a correlated quantum dot sandwiched between the metallic and superconducting leads, considering two types of quenches feasible experimentally. The first one is related to a sudden change of the coupling between the dot and the superconducting lead, while the other one is associated with an abrupt shift of the quantum dot energy level. Using the time-dependent numerical renormalization group method, we examine and quantify the interplay between the proximity induced electron pairing with correlations caused by the on-dot Coulomb repulsion. We determine and discuss the time-dependent charge occupancy, on-dot pair correlation, transient currents, and analyze the evolution of the subgap quasiparticles, which could be empirically observed in the tunneling conductance. To get some insight into the dynamics of a biased junction, we make use of a mean-field approximation. We reveal the signatures of the time-dependent $0-\pi$ transition and demonstrate that the evolution of local observables exhibits damped quantum oscillations with frequencies given by the energies of Andreev bound states.

DOI: [10.1103/PhysRevB.103.155420](https://doi.org/10.1103/PhysRevB.103.155420)

I. MOTIVATION

A quantum impurity (dot) attached to a bulk superconductor can develop the quasiparticle bound states inside the pairing gap $\omega \in (-\Delta, \Delta)$ [1]. These in-gap states originate either from the proximity effect, when the Cooper pairs leak onto this nanoscopic object converting it into superconducting grain, or are driven by the exchange interaction between the quantum dot spin with unpaired electrons of a superconductor. Depending on the specific mechanism, they are dubbed the Andreev [2] or Yu-Shiba-Rusinov bound states [3], respectively. Such in-gap states have been experimentally observed in magnetic atoms and molecules deposited on superconducting substrates [4–7] and in quantum dots embedded into the Josephson [8–10], Andreev [11–13] or multiterminal heterojunctions [14–16].

Recent fast progress of the time-resolved techniques allows us to probe the dynamical properties of these bound states. Several groups have investigated theoretically this issue, inspecting a response time to step-like pulse [17], multiple Andreev (particle-to-hole) reflections [18], sequential tunneling [19], influence of time-dependent bias [20], waiting time distributions [21,22], and short-time counting statistics of the nonequilibrium transport [23]. Moreover, the emergence of metastable bound states in the phase-biased Josephson junction [24,25], transient effects in the Andreev [26] and Josephson [27] circuits, bound states of the periodically driven systems [28–31], cross-correlations between charge currents

in the Cooper-pair-splitter geometry [32–34], and heterostructures with topological superconductors, hosting the Majorana modes [35–37], have also been studied.

Any sudden or smooth change of the model parameters is followed by thermalization processes [38–40]. In the case of superconducting heterostructures such relaxation mechanism requires specifically a continuum electronic spectrum, either from outside the pairing gap Δ [25] or from some additional metallic reservoir [26]. In particular, by abruptly disrupting the quantum system from its ground state the subsequent dynamics may reveal nontrivial behavior upon evolving to its new final state, sometimes undergoing the dynamical quantum phase transitions [41]. The dynamics triggered by such *quantum quench*, when the initial state $|\Psi(t_0)\rangle$ of the Hamiltonian \hat{H}_0 undergoes evolution to $|\Psi(t)\rangle = e^{-i\hat{H}t/\hbar}|\Psi(t_0)\rangle$ of the Hamiltonian $\hat{H}(t > t_0) \neq \hat{H}_0$, has been recently the topic of intensive studies [42]. Such time-dependent phenomena can be conveniently explored in nanoscopic heterostructures, by virtue of the available experimental methods, which enable controllable change of the system's parameters $\hat{H}_0 \rightarrow \hat{H}$.

In this work we study the dynamical properties of the correlated quantum dot (QD) placed between the normal (N) and superconducting (S) electrodes, as schematically sketched in Fig. 1. We focus on two types of quenches, caused by (i) abrupt change of the coupling Γ_S to the superconducting lead and (ii) a sudden alternation of the gate potential, lifting the QD energy level ε_d . We explore the time-dependent signatures of the subgap quasiparticles appearing in the correlated quantum dot. In particular, we examine their behavior in a vicinity of the singlet-doublet quantum phase transition. To accomplish this, we employ the time-dependent numerical renormalization group (tNRG) method [43–45], studying the

*wrzesniewski@amu.edu.pl

†doman@kft.umcs.lublin.pl

‡weymann@amu.edu.pl

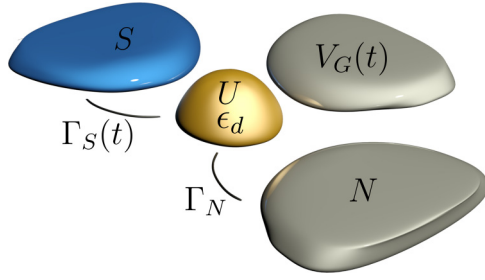


FIG. 1. The considered heterostructure, consisting of a correlated quantum dot (QD), with Coulomb repulsion U and energy level ε_d , coupled to the normal (N) and superconducting (S) leads. The dot's level can be tuned by the gate potential $V_G(t)$.

quench dynamics of unbiased N-QD-S heterostructure. Our calculations for time-dependent observables reveal:

- (i) Quantum oscillations with the period $T = 2\pi/E_A$, where $\pm E_A$ stand for energies of the in-gap quasiparticles,
- (ii) Relaxation rate $2\Gamma_N/\hbar$ appearing in the exponentially decaying amplitudes of these oscillations,
- (iii) Signatures of the dynamical $0-\pi$ transition upon changing the ground state of QD,
- (iv) Competition between the on-dot pairing and the Coulomb repulsion manifested in the time-dependent susceptibility and the QD spin.

Since the verification of these time-dependent phenomena would require measurements of the tunneling currents under nonequilibrium conditions, we have also analyzed the dynamics of the biased N-QD-S heterostructure. Although the tNRG is considered as very accurate and reliable [46], it can be used only at equilibrium. Therefore, to shed some light onto the time-dependent properties of biased junctions, we have adopted a mean-field approach, restricting ourselves to the lowest-order approximation with respect to the Coulomb potential. Under static conditions such an approach has been shown to qualitatively reproduce the transition between the Bardeen-Cooper-Schrieffer (BCS)-type and the singly occupied configurations when varying the coupling Γ_S or the QD energy level ε_d evidenced by a crossing of the bound states [2]. Quantitative results of the lowest and higher-order perturbative treatment are, however, less accurate [47]. We note that, generally, reliable calculations of time-dependent nonequilibrium phenomena of biased quantum dot junctions with strong electron correlations pose a formidable challenge, and there are various sophisticated techniques to accomplish this goal. In particular, this challenging task could be addressed by means of various renormalization group schemes [48–51], continuous time quantum Monte Carlo simulations [52–54], time-resolved density-functional theory [55,56], the continuous unitary transformation technique [57], full counting statistics [24,25,34], Green's functions, and perturbative methods [58–60]. The quench problem can be also described using the conformal field theory and several predictions were successfully confronted with results provided by numerical simulations [61–63]. Therefore, the mean-field results for the time-dependent Andreev conductance presented here should be regarded as providing only the first insight into the nonequilibrium system's behavior, and

might be a starting point for further studies by more reliable methods.

The paper is organized as follows. In Sec. II we formulate the microscopic model, describe the specific quench protocols, and outline two computational methods for determination of the time-dependent physical observables. Next, in Sec. III, we analyze the evolution of the quantum dot occupancy, the on-dot pair correlation and the charge current induced by the quantum quenches in the unbiased hetero-junction. Section IV presents the time-dependent transport properties of the biased system. Finally, in Sec. V we conclude the paper and summarize the main results.

II. FORMULATION OF THE PROBLEM

In this section we present the microscopic model and specify two types of the quantum quenches that could be practically realized. We also outline the computational methods for description of the time-dependent superconducting proximity effect and electron correlations.

A. Microscopic model

The considered N-QD-S heterostructure can be described by the single impurity Anderson Hamiltonian

$$\hat{H} = \underbrace{\sum_{\sigma} \varepsilon_d(t) \hat{d}_{\sigma}^{\dagger} \hat{d}_{\sigma}}_{\hat{H}_{\text{QD}}} + U \hat{n}_{\uparrow} \hat{n}_{\downarrow} + \sum_{\beta} (\hat{H}_{\beta} + \hat{V}_{\beta-\text{QD}}), \quad (1)$$

where \hat{d}_{σ} ($\hat{d}_{\sigma}^{\dagger}$) is the annihilation (creation) operator of the quantum dot electron with spin σ whose (time-dependent) energy is $\varepsilon_d(t)$ and U denotes electrostatic repulsion between the opposite spin electrons. We treat the metallic lead as free fermion gas $\hat{H}_N = \sum_{\mathbf{k},\sigma} \xi_{\mathbf{k}} \hat{c}_{\mathbf{k}\sigma}^{\dagger} \hat{c}_{\mathbf{k}\sigma}$, where $\xi_{\mathbf{k}} = \varepsilon_{\mathbf{k}} - \mu_N$ is the energy $\varepsilon_{\mathbf{k}}$ of itinerant electrons measured from the chemical potential μ_N . The superconducting lead is described by the BCS model $\hat{H}_S = \sum_{\mathbf{q},\sigma} \xi_{\mathbf{q}} \hat{c}_{\mathbf{q}\sigma}^{\dagger} \hat{c}_{\mathbf{q}\sigma} - \sum_{\mathbf{q}} \Delta (\hat{c}_{\mathbf{q}\uparrow}^{\dagger} \hat{c}_{-\mathbf{q}\downarrow}^{\dagger} + \hat{c}_{-\mathbf{q}\downarrow} \hat{c}_{\mathbf{q}\uparrow})$ with energies $\xi_{\mathbf{q}} = \varepsilon_{\mathbf{q}} - \mu_S$ and the isotropic pairing gap Δ .

Coupling of the QD to the metallic lead is given by the hybridization term $\hat{V}_{N-\text{QD}} = \sum_{\mathbf{k},\sigma} (V_{\mathbf{k}} \hat{d}_{\sigma}^{\dagger} \hat{c}_{\mathbf{k}\sigma} + \text{h.c.})$ and $\hat{V}_{S-\text{QD}}$ can be expressed by interchanging the indices $\mathbf{k} \leftrightarrow \mathbf{q}$. We focus here on the in-gap states, therefore for simplicity we can assume the energy-independent couplings $\Gamma_{N(S)} = \pi \sum_{\mathbf{k}(\mathbf{q})} |V_{\mathbf{k}(\mathbf{q})}|^2 \delta(\omega - \varepsilon_{\mathbf{k}(\mathbf{q})})$. For $|\omega| \ll \Delta$, the coupling Γ_S can be regarded as the proximity induced pairing potential, whereas Γ_N controls the inverse life-time of the in-gap quasiparticles. As we shall see, these couplings manifest themselves in the dynamical quantities in qualitatively different ways.

B. Quench protocols

The quantum quench can be in general represented by the following time-dependent Hamiltonian

$$\hat{H}(t) = \theta(-t) \hat{H}_0 + \theta(t) \hat{H}, \quad (2)$$

where $\theta(t)$ is the step function. The initial Hamiltonian \hat{H}_0 is replaced (at time $t = 0$) by another Hamiltonian \hat{H} . In particular, this abrupt change can be realized within the same structure of the model (1) modifying only its parameters.

The expectation value of an arbitrary observable $\hat{O}(t)$ can be then expressed as (for the time-independent Hamiltonian)

$$\begin{aligned} O(t) &\equiv \langle \hat{O}(t) \rangle \\ &= \text{Tr}\{e^{-i\hat{H}t} \hat{\rho}_0 e^{i\hat{H}t} \hat{O}\} \\ &= \text{Tr}\{\hat{\rho}_0 \hat{O}_H(t)\} \\ &\equiv \langle \hat{O}_H(t) \rangle, \end{aligned} \quad (3)$$

where $\hat{\rho}_0$ denotes the initial equilibrium density matrix of the system described by \hat{H}_0 and $\hat{O}_H(t)$ is the Heisenberg representation of \hat{O} .

We shall examine the dynamical behavior of various quantities, considering two different types of quantum quenches. In the first case, we impose an abrupt change of the coupling to superconducting lead

$$V_q(t) = \begin{cases} 0 & \text{for } t \leq 0 \\ V_q & \text{for } t > 0, \end{cases} \quad (4)$$

which is formally equivalent to the assumption $\Gamma_S(t) = \Gamma_S \theta(t)$. The second quantum quench refers to the time-dependent QD energy level

$$\varepsilon_d(t) = \begin{cases} \varepsilon_d & \text{for } t \leq 0 \\ \varepsilon_d + V_G & \text{for } t > 0, \end{cases} \quad (5)$$

and it can be practically achieved by applying the gate potential $V_G(t) = V_G \theta(t)$. Although in both considered quenches the system evolves according to the same final Hamiltonian, we shall see that different initial conditions strongly affect the transient behavior. For computing the time-dependent expectation values of our interest, such as the QD occupancy $n_\sigma(t) \equiv \langle \hat{d}_\sigma^\dagger(t) \hat{d}_\sigma(t) \rangle$, the induced pairing $\chi(t) \equiv \langle \hat{d}_\downarrow(t) \hat{d}_\uparrow(t) \rangle$ and the charge currents $j_{S,N}(t)$ we use two techniques, briefly outlined below.

C. Equation of motion approach

In the absence of interactions ($U=0$) one can exactly determine all required observables, solving the set of coupled equations of motion for appropriate operators. Yet, even for $U=0$, the observables exhibit nontrivial evolution. For an abrupt switch on of the coupling of uncorrelated QD to both external electrodes we have previously determined the characteristic time scales of the subgap bound states [26,27]. Technically, one has to solve the Heisenberg equation of motion of the localized $\hat{d}_\sigma^{(\dagger)}$ and itinerant $\hat{c}_{\mathbf{k}/q\sigma}^{(\dagger)}$ electron operators, respectively. To accomplish this, we have expressed these equations of motion by introducing the Laplace transforms $\hat{O}(s) = \int_0^\infty e^{-st} \hat{O}(t) dt$, which are useful for considering the specific initial conditions $\hat{O}(0)$. Next, computing the inverse Laplace transforms we have determined the time-dependent operators $\hat{O}(t)$ and derived analytical expressions for the needed expectation values, such as $n_\sigma(t) \equiv \langle \hat{d}_\sigma^\dagger(t) \hat{d}_\sigma(t) \rangle$.

A typical evolution of the uncorrelated QD spectrum induced after switching on the coupling $\Gamma_S(t)$ is illustrated in Fig. 2. Initially, the dot is described by energy level ε_d , the broadening (inverse lifetime) of which is equal to $2\Gamma_N$. After attaching the superconductor this quasiparticle state evolves into a pair of Andreev bound states that develop at $\pm E_A$. For $U=0$ and $\Delta \rightarrow \infty$, the energy of Andreev states is given

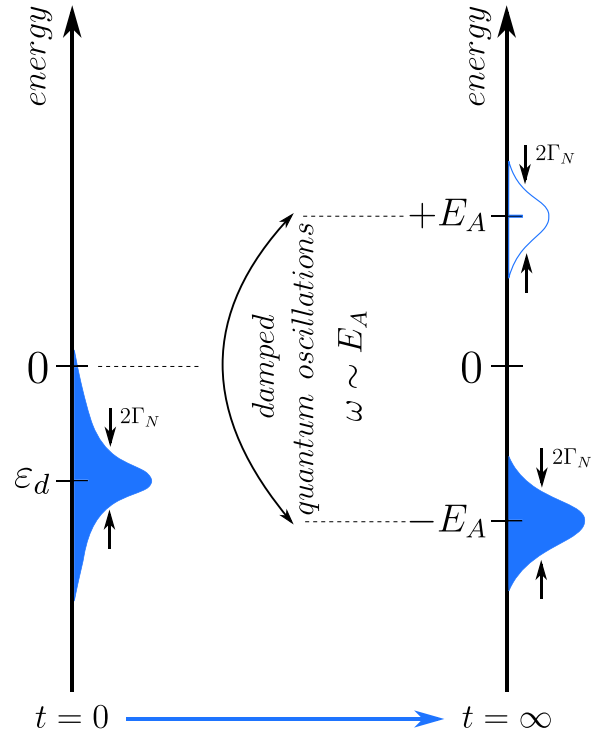


FIG. 2. The illustration of the post-quench evolution driven by a sudden change of the coupling to superconductor $\Gamma_S(t) = \Gamma_S \theta(t)$, presenting the quasiparticle peak existing till $t=0$ at ε_d , which changes into a pair of Andreev bound states at $\pm E_A$. Such changeover is accompanied with damped quantum oscillations of frequency $\omega = E_A$.

by $E_A = \sqrt{\varepsilon_d^2 + \Gamma_S^2}$. Interestingly, such a quasiparticle spectrum is gradually developed through a sequence of quantum oscillations of characteristic frequency $\omega = E_A$, in a fashion reminiscent of the Rabi-type oscillations.

To prove it explicitly, let us consider the effective Hamiltonian $\hat{H} = \sum_\sigma \varepsilon_d \hat{d}_\sigma^\dagger \hat{d}_\sigma + (\Gamma_S \hat{d}_\uparrow^\dagger \hat{d}_\downarrow^\dagger + \text{h.c.})$ in the absence of interactions $U=0$ and neglecting the normal lead $\Gamma_N=0$. Assuming the quantum dot to be initially empty $n_\sigma(0)=0$, we can determine the probability $P(t)$ for inducing the on-dot pair at time $t > 0$ using the standard treatment of two-level systems [64] given by

$$P(t) = \frac{\Gamma_S^2}{\left(\frac{E_1 - E_2}{2}\right)^2 + \Gamma_S^2} \sin^2 \left[t \sqrt{\left(\frac{E_1 - E_2}{2}\right)^2 + \Gamma_S^2} \right]. \quad (6)$$

For the initial energy $E_1=0$ and the final one $E_2=2\varepsilon_d$, we thus obtain the following oscillatory behavior: $P(t) = \left[\frac{\Gamma_S}{E_A} \sin(tE_A) \right]^2$. The additional coupling Γ_N to a continuous spectrum of the normal lead would activate the relaxation processes, responsible for damping.

This approach fails when considering electron interactions, because the corresponding equations of motion cannot be closed. For a weakly correlated system, however, the Coulomb repulsion term can be linearized within the Hartree-Fock-Bogoliubov (HFB) approximation

$$\begin{aligned} \hat{d}_\uparrow^\dagger \hat{d}_\uparrow \hat{d}_\downarrow^\dagger \hat{d}_\downarrow &\simeq n_\uparrow(t) \hat{d}_\downarrow^\dagger \hat{d}_\downarrow + n_\downarrow(t) \hat{d}_\uparrow^\dagger \hat{d}_\uparrow - n_\uparrow(t) n_\downarrow(t) \\ &+ \chi(t) \hat{d}_\uparrow^\dagger \hat{d}_\downarrow^\dagger + \chi^*(t) \hat{d}_\downarrow \hat{d}_\uparrow - |\chi(t)|^2, \end{aligned} \quad (7)$$

and the Hartree-Fock term can be incorporated into the renormalized QD energy level $\tilde{\varepsilon}_d(t) \equiv \varepsilon_d(t) + U n_{-\sigma}(t)$, whereas the anomalous contribution rescales the effective pairing potential $\tilde{\Gamma}_S(t) \equiv \Gamma_S(t) - U \chi(t)$. Unfortunately, the operators $\hat{d}_\sigma(t)$ and $\hat{c}_{k/q\sigma}(t)$ are no longer analytically solvable. In such a case, the expectation values can be computed by solving numerically the set of coupled equations of motion for $n_\sigma(t)$, $\langle \hat{d}_\downarrow(t) \hat{d}_\uparrow(t) \rangle$, $\langle \hat{d}_\sigma^\dagger(t) \hat{c}_{k\sigma}(0) \rangle$, and $\langle \hat{d}_\sigma(t) \hat{c}_{k-\sigma}(t) \rangle$ (see Ref. [26] for details).

Concerning the validity of this mean-field approximation (7), it can be expected to give credible results for the Coulomb potential U smaller than the pairing strength Γ_S . It has been shown [65], that the lowest-order approximation qualitatively reproduces the even-odd parity transition of the proximitized QD, which at half-filling is realized at $U \sim \Gamma_S$. Quantitative comparison of perturbative results with the numerical renormalization group calculations and the quantum Monte Carlo simulations under the stationary conditions has been systematically discussed in Ref. [47]. Nevertheless, as far as real nonequilibrium conditions are concerned, the mean-field approximation should be regarded as giving only the first insight into the system's behavior, while a more accurate analysis of time-dependent properties of biased heterojunctions requires resorting to much more involved methods [48,50,53,56,57].

D. Time-dependent numerical renormalization group

The essential part of our results is obtained by the tNRG technique, which is an extension of the Wilson's numerical renormalization group (NRG) method, suitable for reliable study of the quantum impurity systems at equilibrium [43–46,66,67]. An invaluable advantage of this approach is its very accurate treatment of many-body correlations in a fully nonperturbative manner [46].

For studying the quench dynamics of the time-dependent Hamiltonian (2), we use the NRG method to solve both the initial (\hat{H}_0) and final (\hat{H}) Hamiltonians independently [68]. In the NRG procedure these Hamiltonians are diagonalized in an iterative manner, keeping at each iteration at least N_K energetically lowest-lying eigenstates labeled with superscript K . The discarded high-energy states, labeled with superscript D , are collected from all the iterations and used to construct the full many-body initial and final eigenbases [44]

$$\sum_{nse} |nse\rangle_0^D \langle nse|_0^D = \hat{1} \quad \text{and} \quad \sum_{nse} |nse\rangle^D \langle nse| = \hat{1}, \quad (8)$$

corresponding to \hat{H}_0 and \hat{H} , respectively. The index s labels the eigenstates at iteration with integer number n , while e indicates the environmental subspace representing the rest of the Wilson chain. Here, we note that all eigenstates of the last iteration are considered as discarded. In the next step, an initial full density matrix $\hat{\rho}_0$ is constructed for the system described by \hat{H}_0 at thermal equilibrium [69]

$$\hat{\rho}_0 = \sum_{nse} \frac{e^{-\beta E_{0ns}^D}}{Z} |nse\rangle_0^D \langle nse|_0^D, \quad (9)$$

where $\beta \equiv 1/T$ is the inverse temperature and

$$Z \equiv \sum_{nse} e^{-\beta E_{0ns}^D} \quad (10)$$

is the partition function.

The actual time-dependent calculations are performed in the frequency space. The expectation value of the frequency-dependent local operator $O(\omega) \equiv \langle \hat{O}(\omega) \rangle$ expressed with the use of the corresponding eigenstates is given by

$$O(\omega) = \sum_n^{XX' \neq KK} \sum_{n'} \sum_{ss'}^X |nse\rangle w_{n'} \hat{\rho}_{0n'} |ns'e\rangle^{X'} \times \langle ns'e | \hat{O} | nse \rangle^X \delta(\omega + E_{ns}^X - E_{ns'}^{X'}), \quad (11)$$

where $\hat{\rho}_{0n'}$ is the part of the initial density matrix given at iteration n' and $w_{n'}$ is the weight of the contribution evaluated by tracing out the environmental states [69]. Calculation of the expectation value is performed in an iterative fashion by adding all the contributions, as described in Ref. [70]. Subsequently, the discrete data is weakly smoothed with a log-Gaussian function and broadening parameter $b \leq 0.1$, and then Fourier-transformed into the time domain to eventually obtain a time-dependent expectation value of the local operator [71]

$$O(t) = \int_{-\infty}^{\infty} O(\omega) e^{-i\omega t} d\omega. \quad (12)$$

For our tNRG calculations we have used the discretization parameter $1.5 \leq \Lambda \leq 2$, setting the length of the Wilson chain to $N = 100$ and keeping at least $N_K = 2000$ eigenstates at each iteration. More detailed description of the tNRG implementation in the matrix product state framework has been presented in Ref. [70].

III. DYNAMICS OF UNBIASED SETUP

In this section we analyze the dynamics of unbiased heterojunction, which can be accurately calculated by using the tNRG method. However, for the sake of further analysis, we also present the results obtained with the aid of the mean-field (HFB) approach. In the weak correlation limit, $U \ll \Gamma_S$, we have found that both computational procedures are fairly convergent. In what follows, we present some representative results of the time-dependent quantities, restricting to the superconducting atomic limit $\Delta \rightarrow \infty$. We assume a small coupling to the normal lead, $\Gamma_N = 0.01$, to guarantee long lifetimes of in-gap quasiparticles, what effectively also extends the temporal scale of relaxation processes [26].

Figure 3 shows the time-dependent occupancy $n(t)$, charge current $j_S(t)$ (in units of $\frac{4e}{h} \Gamma_S$) and the real part of the pair correlation $\chi(t)$ obtained for a sudden change of the QD level $\varepsilon_d(t)$. Since the other current $j_N(t)$ obeys the charge conservation law, $j_S(t) + j_N(t) = e \frac{dn(t)}{dt}$, we skip its presentation here. Figure 4 displays the same quantities obtained for a sudden switching of the coupling $\Gamma_S(t) = U \theta(t)$. In both cases we notice that the initial observables gradually evolve to their new steady-state-limit values over the characteristic time interval $\tau \sim 1/\Gamma_N$. Meanwhile, they undergo the quantum oscillations, whose frequency depends on the energies

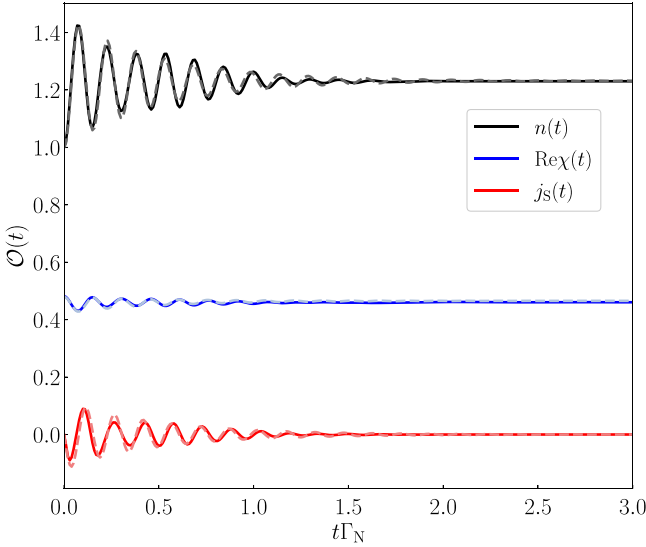


FIG. 3. Comparison of the time-dependent observables obtained by tNRG technique (solid lines) and HFB approximation (dashed lines) for a sudden change of the QD level ε_d from $-U/2$ to $-U$. The couplings of QD to external leads are assumed to be $\Gamma_S = 0.2$, $\Gamma_N = 0.01$ and the Coulomb potential $U = 0.1$ (in units of the band half-width).

of in-gap quasiparticles. This behavior, previously obtained by us analytically for the noninteracting case [26,65,72,73] (Fig. 2), shall be analyzed here focusing on the correlation effects.

Figures 3 and 4 also present a direct comparison of the results obtained by the two approaches. The time-dependent observables calculated by tNRG are presented with the solid lines and the dashed lines display the mean-field approach data. We notice a relatively good qualitative agreement between both methods, albeit a closer inspection reveals the quantitative differences. First of all, the period of quantum oscillations is smaller in tNRG than in the HFB approach. Moreover, the damping of oscillatory behavior obtained within tNRG is more efficient. These differences stem from the fact that correlations give rise to a renormalization of the subgap quasiparticle energies and their lifetimes [74]. This renormalization is not precisely reproduced by HFB approach and such discrepancies would be particularly noticeable in the Kondo regime [72–75] (not discussed here).

A. Quench in coupling Γ_S

To understand the dynamics of the correlated quantum dot driven by an arbitrary quench, it is useful to recall the exact stationary solution for $\Gamma_N = 0$ and $\Delta \rightarrow \infty$. Depending on the model parameters, i.e., ε_d , U and Γ_S , the quantum dot can be either in the singly occupied $|\sigma\rangle$ or the BCS-type $u|0\rangle - v|\uparrow\downarrow\rangle$ ground state [74]. When

$$\left(\varepsilon_d + \frac{U}{2}\right)^2 + \Gamma_S^2 = \left(\frac{U}{2}\right)^2, \quad (13)$$

there occurs a *quantum phase transition* from the (spinful) doublet to the (spinless) singlet configuration. It has crucial importance for an interplay between the on-dot pairing and

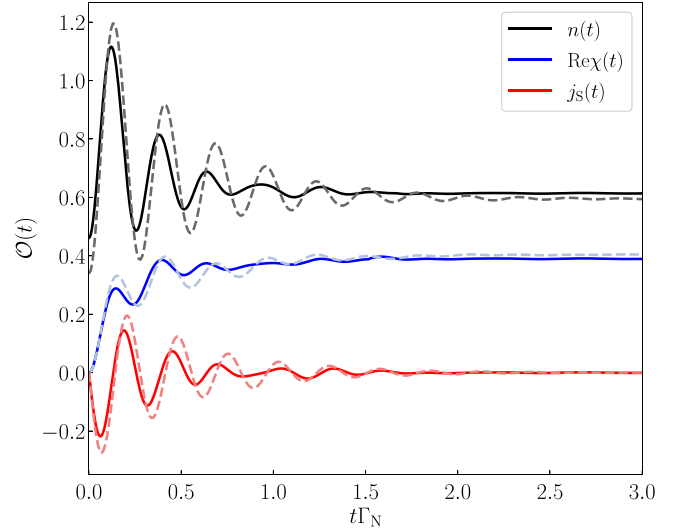


FIG. 4. Comparison of the tNRG results (solid lines) with the mean-field values (dashed lines) obtained for $\varepsilon_d = 0$, $U = 0.1$ and $\Gamma_N = 0.01$ after the quench in Γ_S from zero to its final value $\Gamma_S = U$.

the correlation effects. For the finite coupling $\Gamma_N \neq 0$, such transition is replaced by a crossover, yet the essential features of such distinct singlet/doublet phases are clearly preserved.

For the half-filled QD ($\varepsilon_d = -U/2$) this quantum phase transition (crossover) would occur at $\Gamma_S = U/2$. Figures 5 and 6 present the variation of physical quantities with respect to time (horizontal axis) and the final coupling Γ_S (vertical axis) for the nearly half-filled quantum dot obtained by tNRG and the mean-field approximation, respectively. Again we notice, that in the tNRG results the oscillations are strongly suppressed in comparison to predictions of the mean-field approach. Here, the system is slightly detuned from the particle-hole symmetric point, but QD is still in the Kondo regime characterized by a strong reduction of charge fluctuations. In consequence, the associated current $j_S(t)$ is diminished. As expected, in the doublet region ($\Gamma_S < U/2$) the pair correlation is negligibly small (bottom panel) and we hardly observe any significant charge flow $j_S(t)$ (middle panel) due to the dominant Coulomb repulsion. For stronger couplings $\Gamma_S > U/2$, the quantum dot tends to be in the BCS-type ground state, and this evolution is achieved through damped quantum oscillations (Fig. 5). With increasing Γ_S , the quasiparticle energies move further and further away, therefore the frequency of oscillations increases.

Figures 7 and 8 present the same quantities obtained by tNRG and HFB in the case when QD evolves to the BCS-type configuration for all values of Γ_S . It can be seen that with increasing Γ_S the amplitude of oscillations grows, and so does the frequency. This behavior of N-QD-S setup can be better understood by recalling the Andreev bound state energies [74–76], $\gamma \frac{U}{2} + \eta \sqrt{\xi_d^2 + \Gamma_S^2}$, of the correlated quantum dot obtained in the limit of $\Gamma_N = 0$, where $\xi_d = \varepsilon_d + U/2$ and $\eta, \gamma = \pm 1$. Clearly, the increase of Γ_S changes the quasiparticle energies resulting in larger oscillation frequencies displayed in Figs. 5–8. Using the exact solution in the absence

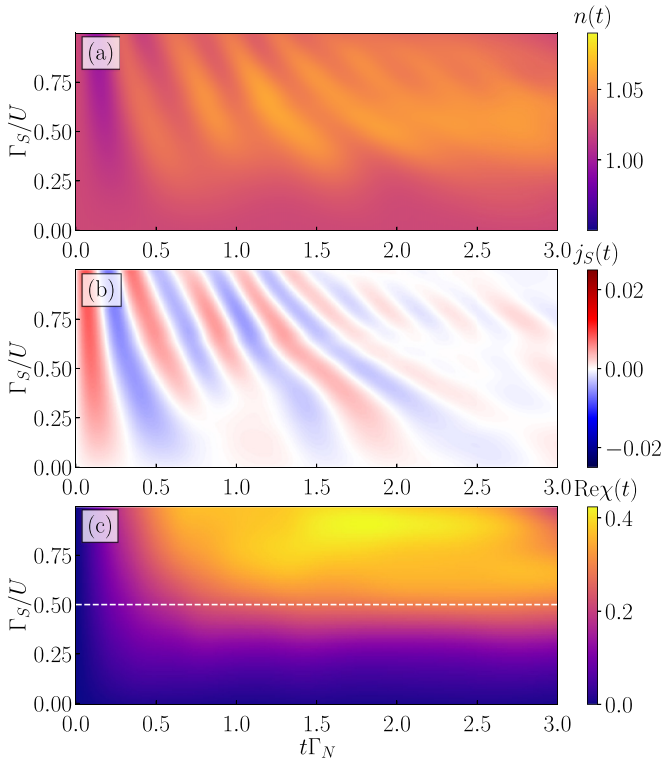


FIG. 5. The time-dependent occupation number $n(t)$, current $j_S(t)$ and real part of the pair correlation $\chi(t) = \langle d_\downarrow(t)d_\uparrow(t) \rangle$ after quench in $\Gamma_S(t)$ from zero to its final value Γ_S (indicated on vertical axis). Results are obtained by tNRG using the model parameters $U = 0.1$, $\Gamma_N = 0.01$ and $\varepsilon_d = -U/2 - \delta$, where $\delta = U/20$.

of relaxation processes (i.e., $\Gamma_N = 0$), we have found the following analytical results:

$$n_\sigma(t) = \frac{\Gamma_S^2}{\xi_d^2 + \Gamma_S^2} \sin^2(t\sqrt{\xi_d^2 + \Gamma_S^2}), \quad (14)$$

$$\text{Re}\chi(t) = \frac{-\xi_d(\Gamma_S/2)}{\xi_d^2 + \Gamma_S^2} \sin^2(t\sqrt{\xi_d^2 + \Gamma_S^2}), \quad (15)$$

$$\text{Im}\chi(t) = \frac{-(\Gamma_S/2)}{\sqrt{\xi_d^2 + \Gamma_S^2}} \sin(2t\sqrt{\xi_d^2 + \Gamma_S^2}). \quad (16)$$

We have assumed here the initially empty quantum dot $n_\sigma(0) = 0$ for the quantum quench of the coupling to superconducting lead from zero to Γ_S . We have checked that such oscillations are in good agreement with the fully self-consistent numerical results obtained for $\Gamma_N \neq 0$.

Comparison between the tNRG and the mean-field results reveals that, most features are qualitatively similar in both methods. Quantitatively, however, there are some differences, as discussed in the previous section.

B. Quench in orbital level position

We now inspect the second type of quantum quench due to abrupt change of the energy level, cf. Eq. (5). Figure 9 presents the time-dependent observables obtained by tNRG for the same parameters as in Fig. 3, assuming $\Gamma_S = 2U$. The orbital level is initially tuned to the particle-hole sym-

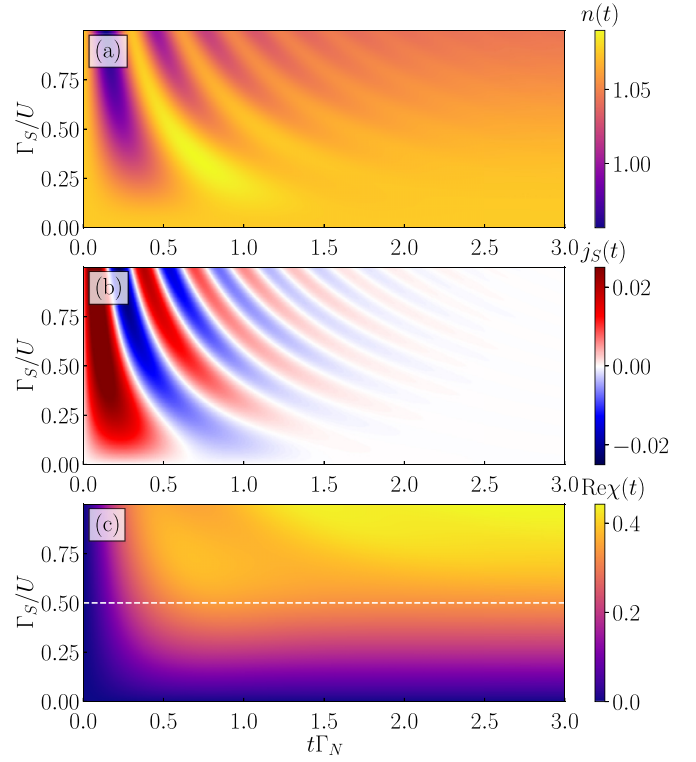


FIG. 6. The mean-field results obtained after the quench of Γ_S for $U = 0.1$, $\Gamma_N = 0.01$, $\varepsilon_d = -U/2 - \frac{U}{20}$ which can be compared to the tNRG data presented in Fig. 5.

metry point, $\varepsilon_d(t \leq 0) = -U/2$, marked by the horizontal dashed line in Fig. 9, and its final value after the quench is indicated on the y axis, correspondingly.

One can see that the evolution of physical observables to their new stationary values is realized through the damped quantum oscillations, analogous to the behavior displayed in Fig. 3. These oscillations show up for a wide range of final values of energy level ε_d . In this regard, the absolute difference $|\varepsilon_d(t \leq 0) - \varepsilon_d(t > 0)|$ affects merely the amplitude of such oscillations. This is especially evident, when examining the time dependence of all observables near the particle-hole symmetry point. For $\varepsilon_d = -U/2$, however, these quantum oscillations completely disappear and we have previously provided physical reasoning for such phenomenon analyzing the transient effects of the uncorrelated system [26]. The oscillations originate from the leakage of Cooper pairs onto the quantum dot and such processes are hardly possible when the initial configuration is exactly half-occupied. Away from the half-filling, the Cooper pairs can flow back and forth, as manifested by the quantum oscillations in all observables. Their frequency depends on the energies E_A of the bound states (see Fig. 2) reminiscent of the Rabi oscillations of two-level quantum systems. The relaxation mechanism originates here from the coupling Γ_N to the continuum spectrum of the metallic lead.

The abrupt change of the QD energy level has a considerable impact on the long-time limit of the charge occupation. For instance, we obtain $n(t \rightarrow \infty) \approx 0.57$ for $\varepsilon_d/U = 0.5$ and $n(t \rightarrow \infty) \approx 1.23$ for $\varepsilon_d/U = -1$, respectively. The oc-

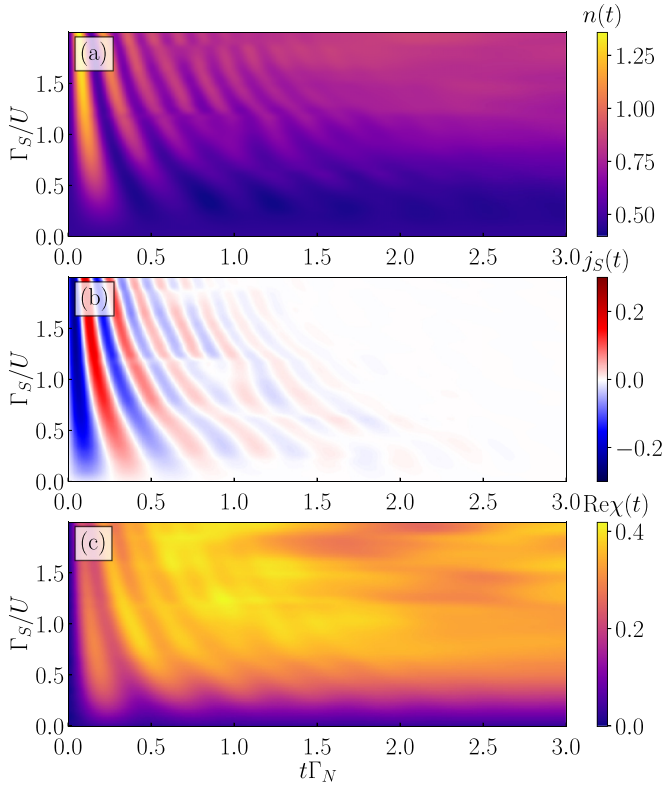


FIG. 7. The time-dependent occupation number $n(t)$, current $j_S(t)$ [in units $\frac{4e}{\hbar}\Gamma_S$] and the real part of $\chi(t) = \langle d_i(t)d_i(t) \rangle$ after the quench in Γ_S (from zero to its finite value indicated in vertical axis). Results are obtained by tNRG for the model parameters $\varepsilon_d = 0$, $U = 0.1$ and $\Gamma_N = 0.01$.

cupancy oscillations are mostly pronounced right after the quench in the early time interval $t\Gamma_N \lesssim 1$. Later on, they are exponentially suppressed with the relaxation rate $\tau \sim 1/\Gamma_N$. Some intriguing effect can be observed in the time-dependent supercurrent $j_S(t)$, whose evolution is characterized by the oscillations shifted by π upon crossing the half-filling $\varepsilon_d = -U/2$. The maxima perfectly coincide with minima around $\varepsilon_d = -U/2$, marked by the dashed lines in Fig. 9. This effect resembles $0 - \pi$ phase transition, whose nature has been widely discussed in the literature for the stationary conditions [47,77]. As already mentioned, the other current $j_N(t)$ is associated with the QD occupancy $n(t)$ and $j_S(t)$ through the charge conservation law $j_S(t) + j_N(t) = e \frac{dn(t)}{dt}$.

The oscillatory behavior after the quench of QD energy level is least evident in the real part of the time-dependent pair correlation $\chi(t)$. This quantity could be regarded as a qualitative measure of the induced on-dot pairing and it indirectly affects the charge current j_N (Sec. IV). Its magnitude is meaningful predominantly in the BCS-type ground state, as evidenced by the NRG studies [74]. The most significant variations of $\text{Re}\chi(t)$ are realized in the short-time limit, when the occupation number $n(t)$ has its minima for quenches to $\varepsilon_d > 0$. We once again recall that when the quantum dot is strongly coupled to superconductor ($\Gamma_S/U = 2$), the large value of $\text{Re}\chi(t)$ firmly establishes in both the initial and final

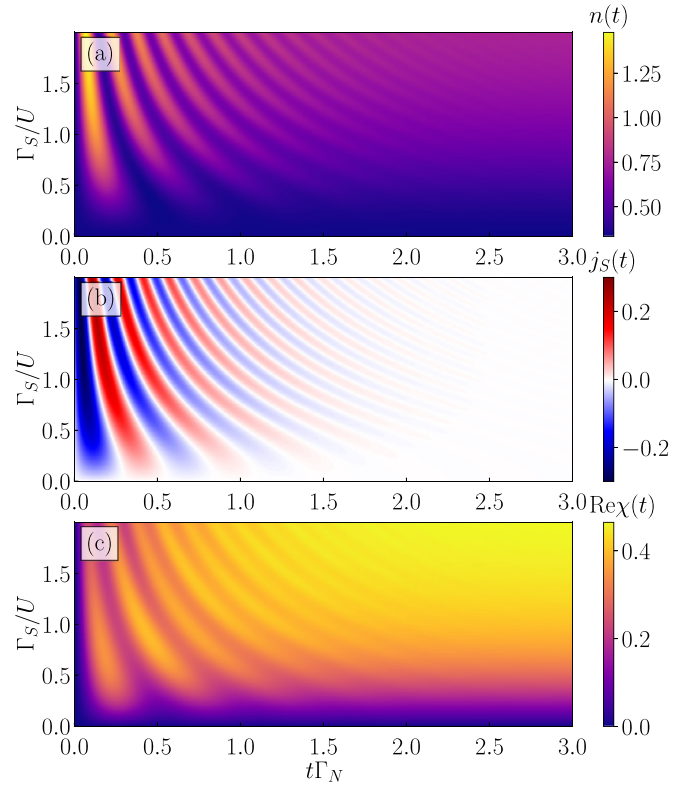


FIG. 8. Evolution of the observables obtained within the mean-field approximation after the quench in Γ_S (from zero to its finite value indicated in vertical axis) for $\varepsilon_d = 0$, $U = 0.1$ and $\Gamma_N = 0.01$. These data can be compared to tNRG results shown in Fig. 7.

states. For this particular regime, the quench does not affect the long-time limit in a considerable way.

Further modifications of the oscillatory time-dependent quantities can be observed when changing the coupling to the superconductor Γ_S . We examine typical results obtained for the N-QD-S setup, using the parameters initially tuned to the quantum phase transition ($\Gamma_S/U = 0.5$). Figure 10 displays the evolution after the quench in the quantum dot energy level, identical to that discussed above. Due to reduction of the coupling Γ_S , the oscillations have lower frequency as compared with the previous case, cf. Eqs. (14)–(16). Additionally, the quench influences the frequency in such way that it is shifted toward higher values as the difference $|\varepsilon_d(t \leq 0) - \varepsilon_d(t > 0)|$ increases. This behavior gives an interesting prospect for a device generating transient supercurrents with the frequency controlled by appropriate switching of the gate potential V_G in a steplike manner. Let us note that the oscillations of the imaginary part of $\chi(t)$ preserve their amplitude. Smaller values of the pairing potential relax the constraints on the long-time limit of the charge occupancy. Here we have, $n(t \rightarrow \infty) \approx 0.2$ for $\varepsilon_d/U = 0.5$ and $n(t \rightarrow \infty) \approx 1.55$ for $\varepsilon_d/U = -1$, thus spanning a wider range of $n(t \rightarrow \infty)$ in comparison with the case of $\Gamma_S/U = 2$ (Fig. 9). On the other hand, the real part of $\chi(t)$ is restricted to a much smaller range, both during the time evolution and after achieving the asymptotics, as expected upon suppressing the pairing amplitude.

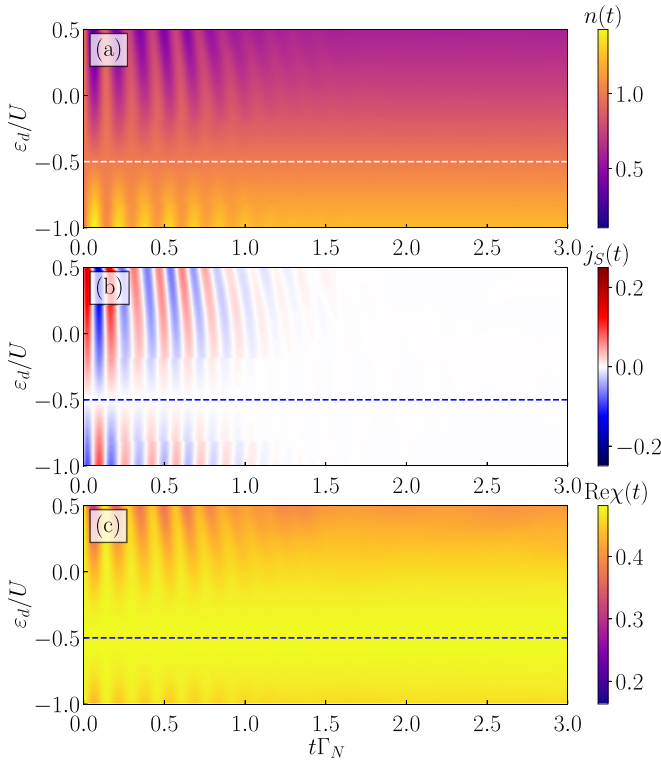


FIG. 9. The time-dependent occupation number $n(t)$, current $j_S(t)$ and the real part of $\langle d_\downarrow(t)d_\uparrow(t) \rangle$ after the quench in QD level ε_d from $-U/2$ to its final value indicated in vertical axis. Results are obtained by tNRG for $\Gamma_S/U = 2$, assuming $U = 0.1$ and $\Gamma_N = 0.01$.

C. Dynamical susceptibility

Dynamical properties of the N-QD-S heterostructure can be further revealed by studying the interplay of the superconducting correlations with the local magnetism. To get an insight into such a competition, let us examine the magnetic susceptibility defined by $\chi_B \equiv \frac{d}{dB} \langle S_z \rangle_{B=0}$, where S_z denotes z -th component of the QD spin. Figure 11 presents the static value of χ_B as a function of temperature T for different couplings Γ_S . In the absence of the superconducting lead ($\Gamma_S = 0$) the maximum of magnetic susceptibility occurs at temperature $T \approx \Gamma_N$. It acquires a reduced value of $\chi_B T \approx 0.19$ as compared to the free-spin case, where $\chi_B T = 1/4$. With decreasing temperature, the Kondo effect comes into play resulting in a full screening of the quantum dot spin for $T/\Gamma_N \lesssim 10^{-3}$, where $\chi_B T \rightarrow 0$. However, when the system is coupled to the superconducting lead, the temperature-dependent susceptibility is substantially modified. As the coupling Γ_S is enhanced, the maximum of susceptibility is reduced and shifted toward higher temperatures. Moreover, the full screening of the orbital level holds at significantly higher temperatures due to the strong superconducting correlations [75]. Finally, for high temperatures, exceeding the values of couplings and Coulomb potential ($T > \Gamma_S, \Gamma_N, U$), all lines converge near $\chi_B T \approx 0.125$.

By varying the coupling strength Γ_S , the most pronounced change of magnetic susceptibility occurs at temperature $T \approx \Gamma_N$. To get an understanding of the dynamical aspects of this dependence, we show in Fig. 12 the time-dependent suscep-

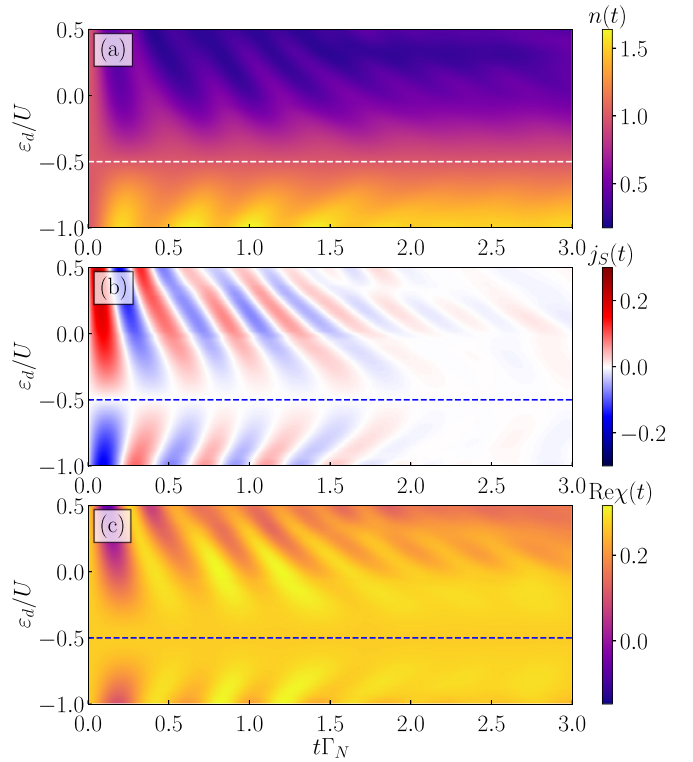


FIG. 10. The time-dependent occupation number $n(t)$, current $j_S(t)$ and the real part of $\langle d_\downarrow(t)d_\uparrow(t) \rangle$ obtained by tNRG after the quench in QD level ε_d from $-U/2$ to its final value indicated in vertical axis for $\Gamma_S/U = 0.5$, $U = 0.1$, $\Gamma_N = 0.01$.

tibility and the squared magnetization after the quench of the coupling Γ_S . Let us remark that magnetic susceptibility (being a measure of a response to external magnetic field) is a property of the system specified in the equilibrium case. Here, we estimate its temporal evolution by calculating the magnetization in a very small but finite external magnetic field B_z , which allows us to approximate the time dependence of the susceptibility as $S_z(t) \approx \chi_B(t)T$.

We consider two initial values of coupling to the superconductor, $\Gamma_S(t < 0)/U = 0.25$ (left column) and $\Gamma_S(t < 0)/U = 0.75$ (right column), associated with the previously discussed spinful and spinless phases, respectively. Let us recall that at the particle-hole symmetry point $\varepsilon_d = -U/2$ the charge and supercurrent dynamics is fully suppressed. We first focus on the case when the evolution is determined after the quench from the spinful configuration with initial value $\Gamma_S(t < 0)/U = 0.25$, see the left column in Fig. 12. When the final value of the coupling strength to superconductor is chosen in such a way that the system remains in the same phase, i.e., $\Gamma_S(t > 0)/U < 0.5$, both $\chi_B(t)$ and $S_z^2(t)$ [panels (a) and (c)] monotonically evolve in a rather moderate manner to a new, slightly modified long-time limit, in agreement with the final thermal expectation values. This regime extends below the cyan dashed lines, indicating a crossover between the phases. However, when $\Gamma_S(t > 0)/U > 0.5$ (values of Γ_S above the cyan line), the system undergoes a transition to the spinless phase and the time dependences reveal a rapid drop of the magnetic properties at time $t\Gamma_S \sim 10^1$. Qualitatively, for the considered system both quantities $\chi_B(t)$ and $S_z^2(t)$

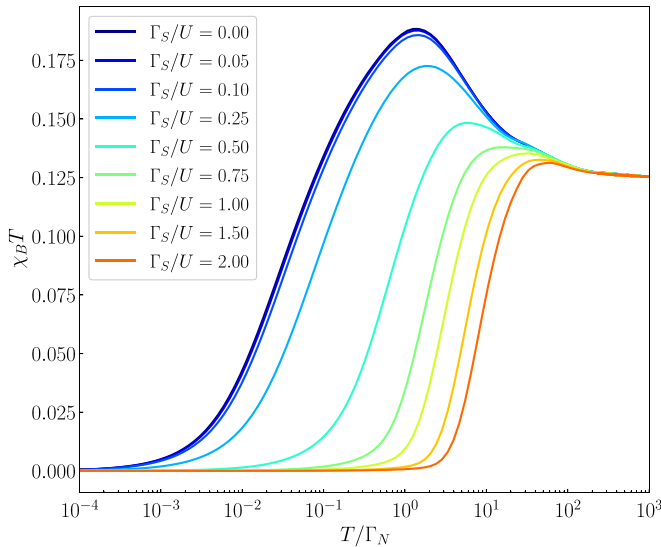


FIG. 11. The magnetic susceptibility as a function of temperature T obtained by NRG for several values of Γ_S , as indicated, for the following parameters: $\varepsilon_d = -U/2$, $\Gamma_N = 0.01$ and $U = 0.1$. Susceptibility is multiplied by temperature T .

have a very similar time dependence and some differences are mainly due to distinct thermal expectation values of the initial and final states. Additionally, the squared magnetization evolves in a smoother manner, while the magnetic susceptibility may undergo weak oscillations at times around $t\Gamma_S \sim 10^2$ before fully relaxing to the new final state. As a reference, in Fig. 12(e) we also show $S_z^2(t)$ evaluated for $T/\Gamma_N \sim 10^{-7}$, which is in good agreement with dependences at higher temperatures. However, $\chi_B(t)$ at $T/\Gamma_N \sim 10^{-7}$ no longer exhibits the discussed behavior due to the full suppression of the magnetic susceptibility at low temperatures, as shown in Fig. 11.

On the other hand, when the dot is in the initial spinless phase and the coupling varies from $\Gamma_S(t < 0)/U = 0.75$ [see the right column in Fig. 12], the response looks significantly different in comparison to the above-discussed case. A striking difference is that here the dynamics is no longer strongly dependent on the coupling Γ_S . To clearly show this effect, we plot the time-dependent expectation values as functions of $t\Gamma_N$. For a relatively small change in the coupling $\Gamma_S(t > 0)/U > 0.5$, i.e., when after the quench the system remains in the spinless phase, the quantities sustain a mild and monotonic evolution toward new thermal limit. However, when the system undergoes a phase transition to the spinful configuration and $\Gamma_S(t > 0)/U < 0.5$ [regime below the cyan dashed line], an enhancement of the magnetic susceptibility and the squared magnetization is considerable. The buildup of $\chi_B(t)$ is noticeable at times $t\Gamma_N \sim 10^0$, revealing similar oscillations as in the case of transition to the opposite direction. Finally, the new asymptotics is achieved at times $10^1 < t\Gamma_N < 10^2$, depending on the magnitude of the quantum quench. The dynamical behavior of $S_z^2(t)$ is again similar to the evaluated time-dependent magnetic susceptibility, but it exhibits suppressed quantum oscillations and the buildup is considerably ahead of $\chi_B(t)$. At times $t\Gamma_N \approx 10^0$, it achieves maximum, which is quickly followed by thermalization to a

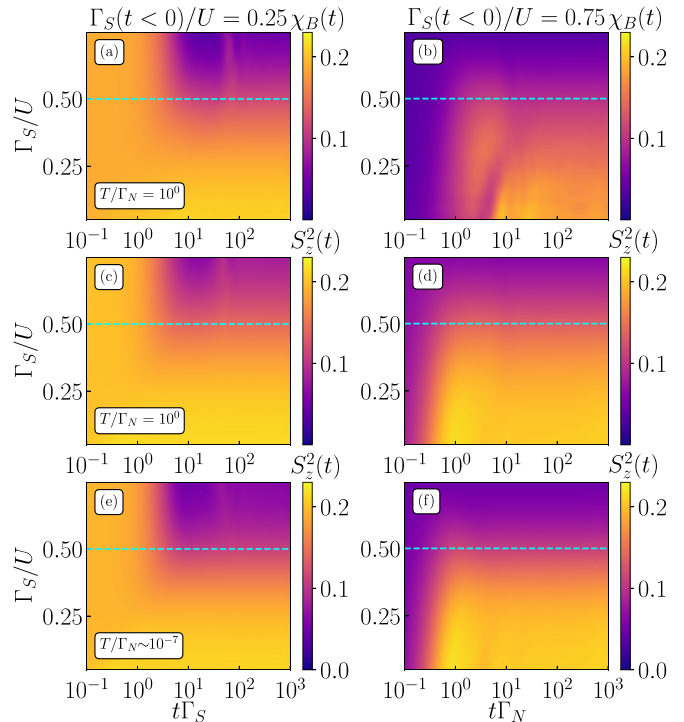


FIG. 12. The time-dependent susceptibility $\chi_B(t)$ and square of the magnetization $S_z^2(t)$ after the quench in Γ_S from initial value indicated at the top of each column. Results shown in (a)–(d) are calculated for temperature $T/\Gamma_N = 10^0$, while (e) and (f) are determined for $T/\Gamma_N \sim 10^{-7}$. Cyan dashed lines indicate the coupling strength $\Gamma_S(t) = U/2$ associated with the quantum phase transition. Results are obtained by tNRG for $\varepsilon_d = -U/2$, $\Gamma_N = 0.01$ and $U = 0.1$.

new value obtained for times $t\Gamma_N \ll 10^1$. Finally, the low temperature behavior of $S_z^2(t)$, see Fig. 12(f), allows one to predict dynamical magnetic behavior of the system at higher temperatures and conversely.

IV. BIASED HETEROJUNCTION

Finally, we briefly discuss the time-dependent charge transport through the N-QD-S heterostructure when the chemical potential μ_N is detuned from μ_S by an applied bias $eV = \mu_N - \mu_S$. For convenience, we assume $\mu_S = 0$. The calculations of time-dependent properties of biased junction are performed by means of the mean-field approach within the Hartree-Fock-Bogoliubov approximation, cf. Eq. (7). We notice that although certain degree of qualitative agreement between the mean-field and tNRG results presented in previous section may trigger optimistic conclusions, the use of the HFB approach for the biased setup should be considered as merely giving the first insight into the out-of-equilibrium system's behavior.

Figure 13 illustrates how the time-dependent current flowing to the superconductor changes with the applied bias voltage. With increasing the bias voltage, one can see that the characteristic current oscillations depart from the particle-hole symmetry point, approximately by the magnitude of the applied voltage $|eV|$. As a consequence, at finite bias, there is a rather constant nonequilibrium current flowing between

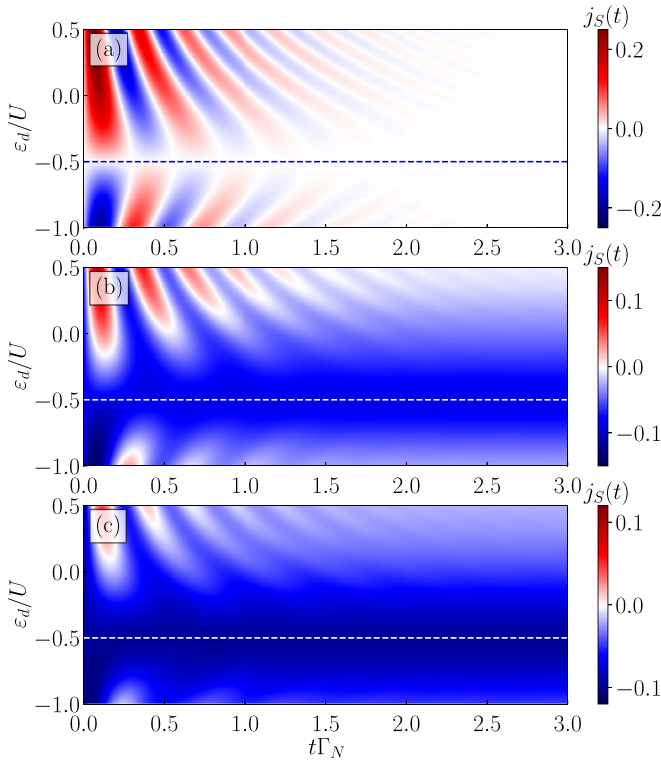


FIG. 13. The time-dependent current $j_S(t)$ obtained within the mean-field approach in the presence of finite bias voltage V . The panels (a), (b), and (c) correspond to $eV/U = 0, -0.5$ and -1.0 , respectively. The model parameters are $\Gamma_S/U = 0.5$, $U = 0.1$, and $\Gamma_N = 0.01$.

the dot and the superconductor, while the time-dependent current oscillations are visible for $\varepsilon_d \gtrsim -U/2 + eV$ and $\varepsilon_d \lesssim -U/2 - eV$, see Fig. 13.

Let us now focus on the differential conductance $G_N(V, t) = \frac{d j_N(t)}{dV}$ of the charge current induced between the quantum dot and the normal lead. We remind that the other current $j_S(t)$ can be inferred from the conservation law $j_S(t) = \frac{dn(t)}{dt} - j_N(t)$. The charge flow from the metallic lead to QD can be formally expressed by the following expectation value: $j_N(t) = e \langle \frac{d}{dt} \sum_{\mathbf{k}, \sigma} \hat{c}_{\mathbf{k}\sigma}^\dagger(t) \hat{c}_{\mathbf{k}\sigma}(t) \rangle$. Determining the time derivative from the equation of motion, one obtains

$$j_N(t) = 2e \sum_{\mathbf{k}, \sigma} \text{Im} \{ V_{\mathbf{k}} \langle \hat{d}_\sigma^\dagger(t) \hat{c}_{\mathbf{k}\sigma}(t) \rangle \}, \quad (17)$$

where the operators of itinerant electrons are governed by $\hat{c}_{\mathbf{k}\sigma}(t) = \hat{c}_{\mathbf{k}\sigma}(0) e^{-i\epsilon_{\mathbf{k}} t} - i \int_0^t dt' V_{\mathbf{k}} e^{-i\epsilon_{\mathbf{k}}(t-t')} \hat{d}_\sigma(t')$ [26]. The remaining computational difficulty is related here with the time-dependent operators $\hat{d}_\sigma^\dagger(t)$. These operators can be determined, depending on specific quantum quench, from the equation of motion algorithm described in detail by us for the uncorrelated N-QD-S heterostructure in Ref. [26] (see Appendix A.1 therein). Our study addresses the subgap transport driven by bias voltage V , smaller than the pairing gap Δ , which in conventional superconductors is on the order of meV. Otherwise, one should resort to more sophisticated methods to deal with the time-dependent transport phenomena under nonequilibrium conditions in the presence of correlations, e.g., exploiting symmetries, fluctuation relations and/or dualities [78–80].

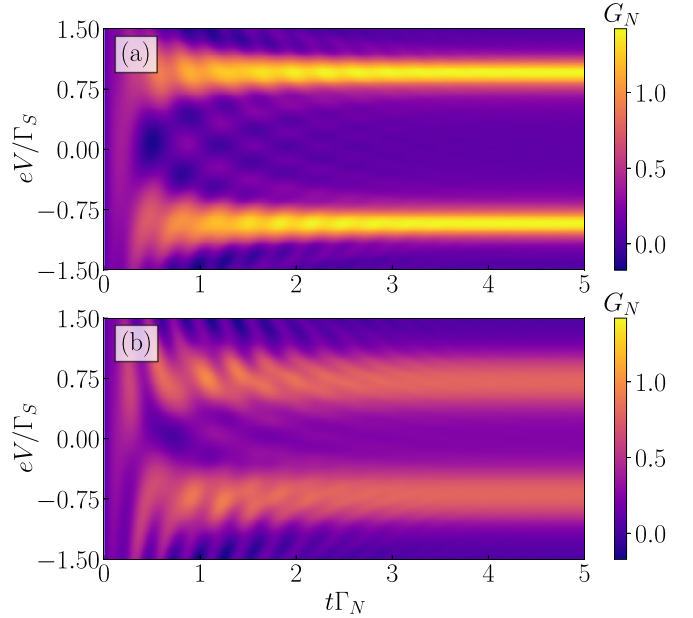


FIG. 14. Variation of the differential conductance G_N (in units of $2e^2/h$) with respect to voltage V and time t obtained by the mean-field approximation after a sudden coupling of the QD to external leads at $t = 0^+$ for $\Gamma_N = 0.01$, $\Gamma_S = 0.1$, $\varepsilon_d = -U/2$ and assuming (a) $U = 0.025$, (b) $U = 0.1$.

The steady-state limit current $j_N(\infty)$ can be independently determined, for instance, from the Landauer formalism. Such Andreev-type spectroscopy has been widely discussed in the literature [2,3]. Here, we are mainly interested in the time evolution of the tunneling current $j_N(t)$ towards its steady-state limit, which encompasses the relaxation processes (imposed by the coupling Γ_N) and the quantum oscillations with frequencies sensitive to the ratio of Γ_S/U and dependent on the QD level ε_d .

We first consider the situation when at $t = 0^+$ the QD is simultaneously coupled to the both external leads. Under such circumstances, we can observe signatures of the emerging bound states, manifested in the time-dependent differential conductance $G_N(V, t)$. Figure 14 presents these transient effects for several model parameters ε_d , Γ_S , U (as indicated). The plots clearly show gradual buildup of the in-gap states at energies $\pm E_A$ characterized either by the symmetric (for $\varepsilon_d = -U/2$) or asymmetric spectral weights (away from the half-filling). These features are well established around $t \sim 1/\Gamma_N$ and until such time, the transient behavior reveals the quantum oscillations with the period given by $2\pi/E_A$.

Let us now focus on the quantum quenches described by Eqs. (4) and (5). Figure 15 displays the differential conductance obtained for the half-filled QD ($\varepsilon_d = -U/2$) suddenly attached to the superconducting lead. We set the Coulomb potential $U = 0.1$ and impose the quench $\Gamma_S(t) = U\theta(t)$. Initially, the normal quantum dot is characterized by the quasiparticle peaks at energies ε_d and $\varepsilon_d + U$, which for the half-filled QD occur at $\pm U/2$. The superconducting proximity effect drives the quantum dot to the new quasiparticle states, cf. Eqs. (14)–(16). The emergence of such new quasiparticles resembles the transient phenomena presented in Fig. 14. This

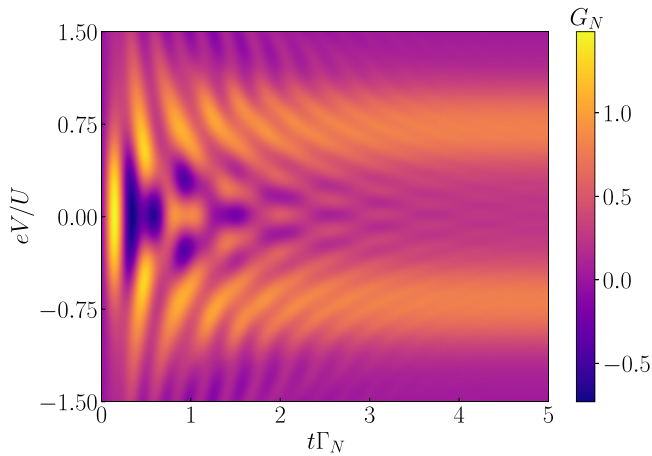


FIG. 15. The differential conductance G_N as a function of voltage (vertical axis) and time (horizontal axis) after the quench in Γ_S from zero to 0.1 obtained by the mean-field calculations for $\Gamma = 0.01$, $U = 0.1$ and $\varepsilon_d = -U/2$.

is rather not surprising, considering the fact that Γ_N is much weaker as compared to Γ_S and U .

Figure 16 shows $G_N(V, t)$ after the quench of QD level from $\varepsilon_d(t \leq 0) = -U/2$ to $\varepsilon_d(t > 0) = U/2$. In this figure we have assumed $\Gamma_S = U$, guaranteeing that at the initial and final stages the quantum dot is safely in the BCS-type configuration. A sudden change of the energy level is responsible for the modification of the energies of subgap quasiparticles $\pm E_A$ and inducing asymmetry of their spectral weights.

Finally, we discuss the evolution of the quasiparticle spectra manifesting transitions between the singlet and doublet configurations. Such a situation can be achieved in two steps, as displayed in Fig. 17. Initially, at $t = 0^+$, the half-filled quantum dot is coupled to both electrodes, with $\Gamma_S > U/2$ (upper panel) and $\Gamma_S < U/2$ (bottom panel). We analyze the transient effects in the time interval $t \in (0, 5/\Gamma_N)$. Next, for $t = 5/\Gamma_N$, we abruptly reverse these couplings. Such change triggers transitions from the doublet to singlet phase (upper panel) and from the singlet to doublet phase (bottom panel), respectively. We notice that the postquench behavior is not

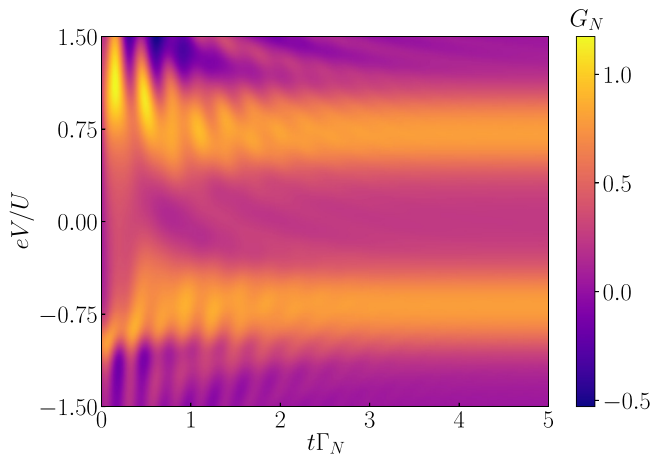


FIG. 16. The differential conductance G_N obtained by mean-field approach for $\Gamma_N = 0.01$ and $\Gamma_S/U = 1$, imposing a sudden change of the QD energy level $\varepsilon_d = U/2 \rightarrow -U/2$.

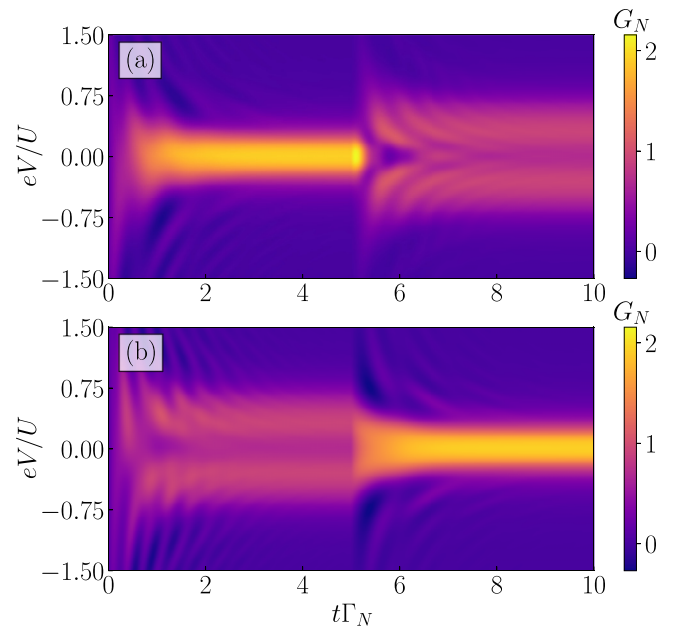


FIG. 17. The differential conductance G_N calculated by the mean-field approach across the doublet-singlet transition driven by the quench in Γ_S : from 0.03 up to 0.07 (upper panel) and from 0.07 down to 0.03 (bottom panel). The quench was imposed at $t = 5/\Gamma_N$ using the model parameters: $\Gamma_N = 0.01$, $U = 0.1$ and $\varepsilon_d = -U/2$.

completely identical in both cases, but the quasiparticle features in the upper/bottom panel right before the quench are pretty similar to the asymptotic quasiparticle features visible in the bottom/upper panels.

V. SUMMARY AND OUTLOOK

We have studied the dynamical properties of the correlated quantum dot coupled to the metallic and superconducting leads, considering two quantum quenches driven by (a) a sudden shift of the energy level and (b) an abrupt change of the coupling between the quantum dot and the superconductor. To accurately treat the correlation effects, we have used the time-dependent numerical renormalization group method to study the dynamics of an unbiased junction. For both types of quantum quenches, we have observed that the time-dependent observables (such as quantum dot charge, induced on-dot pairing, and local currents) gradually evolve to their stationary-limit values through a series of damped quantum oscillations. The frequencies of these oscillations coincide with the energies of the in-gap quasiparticles, whereas the relaxation rate depends on the strength of coupling to metallic lead Γ_N . These findings are summarized in Fig. 18 for representative values of Γ_N/U ratio, showing that the amplitude of quantum oscillations is indeed governed by an envelope function $e^{-t/\tau}$ with the characteristic time scale $\tau = (2\Gamma_N)^{-1}$.

We have also considered two specific realizations of quantum quenches, inducing a changeover of the quantum dot ground state between the singlet and doublet (spinless and spinful) configurations. Traversing from the BCS-type to the doublet configuration (and *vice versa*), we have found a π shift in the time-dependent charge current $j_S(t)$ flowing from the superconductor to the quantum dot. This phenomenon can be

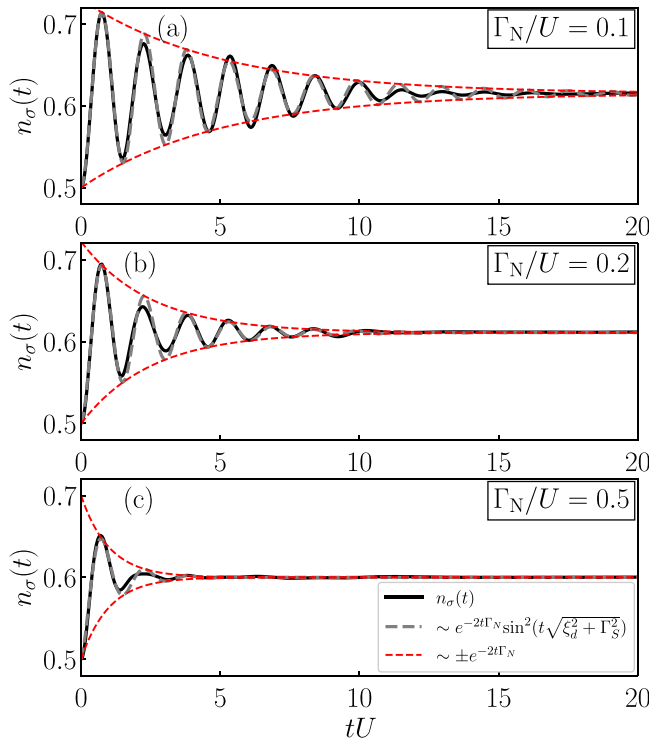


FIG. 18. Variation of $n_\sigma(t)$ induced by shifting the QD energy level ε_d from $-U/2$ to $-U$ for several couplings Γ_N (as indicated). Solid lines display the tNRG results, thick-dashed (gray) curves refer to $e^{-2t\Gamma_N} \sin^2(t\sqrt{\xi_d^2 + \Gamma_S^2})$ and thin-dashed (red) lines present the exponential envelope function. Results are obtained for $\Gamma_S = 0.2$ and $U = 0.1$.

regarded as the dynamical signature of the $0 - \pi$ transition, widely studied in the stationary charge transport through a correlated quantum dot embedded in the Josephson-type junction [2,65,77].

Furthermore, we have predicted qualitative changes of the time-dependent magnetic properties upon approaching the quantum phase transition after the quench of either the energy level ε_d or the coupling Γ_S . The dynamical susceptibility and the squared quantum dot spin clearly reveal a

competition between the on-dot pairing and the Coulomb correlations. Signatures of such competition are manifested in the time-dependent on-dot pairing, which is empirically accessible through the subgap tunneling spectroscopy. For this reason, we have also investigated the nonequilibrium charge transport of the biased N-QD-S nanostructure by using the mean-field approach with respect to the Coulomb repulsion. We have shown that the time- and voltage-dependent Andreev conductance reveals all qualitative details of the subgap quasiparticles. Consequently, studying the quantum quenches allows for a precise identification of the energies, lifetimes and other (for instance magnetic) properties of the subgap quasiparticles.

Finally, we find it of importance to make a comment on the methodology used in this paper. For the dynamics of unbiased heterostructure we have used the very accurate time-dependent numerical renormalization group method. The numerical results obtained by this method can be considered as very reliable. On the other hand, to get some insight into the system dynamics in the case of finite bias voltage, the case which cannot be captured by tNRG, we have resorted to the mean-field method, which is however much less accurate. Because the mean-field calculations of the charge transport can be considered as reliable only for weakly correlated systems, our HFB results should be viewed as providing some first insights into the time-dependent properties of the biased junction. In this regard, we note that it would be worthwhile to reexamine the dynamical effects of the strongly correlated N-QD-S nanostructure under nonequilibrium conditions in future studies by employing more reliable methods [48,50,53,56,57,63].

ACKNOWLEDGMENTS

This work is supported by the National Science Centre (Poland) under Grants No. 2018/29/N/ST3/01038 (K.W.), No. 2017/27/B/ST3/00621 (I.W.), No. 2017/27/B/ST3/01911 (B.B. and R.T.), and No. 2018/29/B/ST3/00937 (T.D.).

- [1] A. V. Balatsky, I. Vekhter, and J.-X. Zhu, Impurity-induced states in conventional and unconventional superconductors, *Rev. Mod. Phys.* **78**, 373 (2006).
- [2] A. Martín-Rodero and A. Levy Yeyati, Josephson and Andreev transport through quantum dots, *Adv. Phys.* **60**, 899 (2011).
- [3] V. Koerting, B. M. Andersen, K. Flensberg, and J. Paaske, Nonequilibrium transport via spin-induced subgap states in superconductor/quantum dot/normal metal cotunnel junctions, *Phys. Rev. B* **82**, 245108 (2010).
- [4] A. Yazdani, B. A. Jones, C. P. Lutz, M. F. Crommie, and D. M. Eigler, Probing the local effects of magnetic impurities on superconductivity, *Science* **275**, 1767 (1997).
- [5] S.-H. Ji, T. Zhang, Y.-S. Fu, X. Chen, X.-C. Ma, J. Li, W.-H. Duan, J.-F. Jia, and Q.-K. Xue, High-Resolution Scanning Tunneling Spectroscopy of Magnetic Impurity Induced

Bound States in the Superconducting Gap of Pb Thin Films, *Phys. Rev. Lett.* **100**, 226801 (2008).

- [6] K. J. Franke, G. Schulze, and J. I. Pascual, Competition of superconducting phenomena and Kondo screening at the nanoscale, *Science* **332**, 940 (2011).
- [7] B. W. Heinrich, J. I. Pascual, and K. J. Franke, Single magnetic adsorbates on s-wave superconductors, *Prog. Surf. Sci.* **93**, 1 (2018).
- [8] S. De Franceschi, L. Kouwenhoven, C. Schönberger, and W. Wernsdorfer, Hybrid superconductor–quantum dot devices, *Nat. Nanotech.* **5**, 703 (2010).
- [9] R. Maurand, T. Meng, E. Bonet, S. Florens, L. Marty, and W. Wernsdorfer, First-Order $0-\pi$ Quantum Phase Transition in the Kondo Regime of a Superconducting Carbon-Nanotube Quantum Dot, *Phys. Rev. X* **2**, 011009 (2012).

- [10] A. García Corral, D. M. T. van Zanten, K. J. Franke, H. Courtois, S. Florens, and C. B. Winkelmann, Magnetic-field-induced transition in a quantum dot coupled to a superconductor, *Phys. Rev. Research* **2**, 012065(R) (2020).
- [11] R. S. Deacon, Y. Tanaka, A. Oiwa, R. Sakano, K. Yoshida, K. Shibata, K. Hirakawa, and S. Tarucha, Kondo-enhanced Andreev transport in single self-assembled InAs quantum dots contacted with normal and superconducting leads, *Phys. Rev. B* **81**, 121308(R) (2010).
- [12] J. Schindele, A. Baumgartner, and C. Schönenberger, Near-Unity Cooper Pair Splitting Efficiency, *Phys. Rev. Lett.* **109**, 157002 (2012).
- [13] E. J. H. Lee, X. Jiang, M. Houzet, R. Aguado, C. M. Lieber, and S. De Franceschi, Spin-resolved Andreev levels and parity crossings in hybrid superconductor-semiconductor nanostructures, *Nat. Nano* **9**, 79 (2014).
- [14] J. Schindele, A. Baumgartner, R. Maurand, M. Weiss, and C. Schönenberger, Nonlocal spectroscopy of Andreev bound states, *Phys. Rev. B* **89**, 045422 (2014).
- [15] A. P. Higginbotham, S. M. Albrecht, G. Kiršanskas, W. Chang, F. Kuemmeth, P. Krogstrup, T. S. Jespersen, J. Nygard, K. Flensberg, and C. M. Marcus, Parity lifetime of bound states in a proximitized semiconductor nanowire, *Nat. Phys.* **11**, 1017 (2015).
- [16] J. Gramich, A. Baumgartner, and C. Schönenberger, Andreev bound states probed in three-terminal quantum dots, *Phys. Rev. B* **96**, 195418 (2017).
- [17] Y. Xing, Q.-F. Sun, and J. Wang, Response time of a normal-metal/superconductor hybrid system under a step-like pulse bias, *Phys. Rev. B* **75**, 125308 (2007).
- [18] G. Stefanucci, E. Perfetto, and M. Cini, Time-dependent quantum transport with superconducting leads: A discrete-basis Kohn-Sham formulation and propagation scheme, *Phys. Rev. B* **81**, 115446 (2010).
- [19] L. D. Contreras-Pulido, J. Splettstoesser, M. Governale, J. König, and M. Büttiker, Time scales in the dynamics of an interacting quantum dot, *Phys. Rev. B* **85**, 075301 (2012).
- [20] E. K. U. Gross and K. J. Pototzky, Controlling observables in time-dependent quantum transport, [arXiv:1407.2554](https://arxiv.org/abs/1407.2554).
- [21] L. Rajabi, C. Pörtl, and M. Governale, Waiting Time Distributions for the Transport Through a Quantum-Dot Tunnel Coupled to One Normal and One Superconducting Lead, *Phys. Rev. Lett.* **111**, 067002 (2013).
- [22] G. Michałek, B. R. Bułka, T. Domański, and K. I. Wysokiński, Statistics of tunneling events in three-terminal hybrid devices with quantum dot, *Acta Phys. Polon. A* **133**, 391 (2018).
- [23] P. Stegmann and J. König, Short-time counting statistics of charge transfer in Coulomb-blockade systems, *Phys. Rev. B* **94**, 125433 (2016).
- [24] R. S. Souto, A. Martín-Rodero, and A. Levy Yeyati, Andreev Bound States Formation and Quasiparticle Trapping in Quench Dynamics Revealed by Time-Dependent Counting Statistics, *Phys. Rev. Lett.* **117**, 267701 (2016).
- [25] R. S. Souto, A. Martín-Rodero, and A. Levy Yeyati, Quench dynamics in superconducting nanojunctions: Metastability and dynamical Yang-Lee zeros, *Phys. Rev. B* **96**, 165444 (2017).
- [26] R. Taranko and T. Domański, Buildup and transient oscillations of Andreev quasiparticles, *Phys. Rev. B* **98**, 075420 (2018).
- [27] R. Taranko, T. Kwapiński, and T. Domański, Transient dynamics of a quantum dot embedded between two superconducting leads and a metallic reservoir, *Phys. Rev. B* **99**, 165419 (2019).
- [28] K. F. Albrecht, H. Soller, L. Mühlbacher, and A. Komnik, Transient dynamics and steady state behavior of the Anderson-Holstein model with a superconducting lead, *Physica E* **54**, 15 (2013).
- [29] R. Mélin, J.-G. Caputo, K. Yang, and B. Douçot, Simple Floquet-Wannier-Stark-Andreev viewpoint and emergence of low-energy scales in a voltage-biased three-terminal Josephson junction, *Phys. Rev. B* **95**, 085415 (2017).
- [30] L. Arrachea and R. López, Anomalous Joule law in the adiabatic dynamics of a quantum dot in contact with normal-metal and superconducting reservoirs, *Phys. Rev. B* **98**, 045404 (2018).
- [31] B. Baran and T. Domański, Quasiparticles of a periodically driven quantum dot coupled between superconducting and normal leads, *Phys. Rev. B* **100**, 085414 (2019).
- [32] K. Wrześniewski and I. Weymann, Current cross-correlations and waiting time distributions in Andreev transport through Cooper pair splitters based on a triple quantum dot system, *Phys. Rev. B* **101**, 155409 (2020).
- [33] N. Walldorf, F. Brange, C. Padurariu, and Ch. Flindt, Noise and full counting statistics of a Cooper pair splitter, *Phys. Rev. B* **101**, 205422 (2020).
- [34] G. Michałek, B. R. Bułka, T. Domański, and K. I. Wysokiński, Statistical correlations of currents flowing through a proximitized quantum dot, *Phys. Rev. B* **101**, 235402 (2020).
- [35] R. Seoane Souto, K. Flensberg, and M. Leijnse, Timescales for charge transfer based operations on Majorana systems, *Phys. Rev. B* **101**, 081407(R) (2020).
- [36] T. Jonckheere, J. Rech, A. Zazunov, R. Egger, A. L. Yeyati, and T. Martin, Giant Shot Noise from Majorana Zero Modes in Topological Trijunctions, *Phys. Rev. Lett.* **122**, 097003 (2019).
- [37] J. Manousakis, C. Wille, A. Altland, R. Egger, K. Flensberg, and F. Hassler, Weak Measurement Protocols for Majorana Bound State Identification, *Phys. Rev. Lett.* **124**, 096801 (2020).
- [38] A. Polkovnikov, K. Sengupta, A. Silva, and M. Vengalattore, Colloquium: Nonequilibrium dynamics of closed interacting quantum systems, *Rev. Mod. Phys.* **83**, 863 (2011).
- [39] H. Fotso, K. Mikelsons, and J. K. Freericks, Thermalization of field driven quantum systems, *Sci. Rep.* **4**, 4699 (2014).
- [40] I. Weymann, J. von Delft, and A. Weichselbaum, Thermalization and dynamics in the single-impurity Anderson model, *Phys. Rev. B* **92**, 155435 (2015).
- [41] M. Heyl, Dynamical quantum phase transitions: a review, *Rep. Prog. Phys.* **81**, 054001 (2018).
- [42] A. Mitra, Quantum quench dynamics, *Annu. Rev. Condens. Matter Phys.* **9**, 245 (2016).
- [43] K. G. Wilson, The renormalization group: Critical phenomena and the Kondo problem, *Rev. Mod. Phys.* **47**, 773 (1975).
- [44] F. B. Anders and A. Schiller, Real-Time Dynamics in Quantum-Impurity Systems: A Time-Dependent Numerical Renormalization-Group Approach, *Phys. Rev. Lett.* **95**, 196801 (2005).
- [45] F. B. Anders and A. Schiller, Spin precession and real-time dynamics in the Kondo model: Time-dependent numerical renormalization-group study, *Phys. Rev. B* **74**, 245113 (2006).

- [46] R. Bulla, T. A. Costi, and T. Pruschke, Numerical renormalization group method for quantum impurity systems, *Rev. Mod. Phys.* **80**, 395 (2008).
- [47] A. Kadlecová, M. Žonda, V. Pokorný, and T. Novotný, Practical Guide to Quantum Phase Transitions in Quantum-Dot-Based Tunable Josephson Junctions, *Phys. Rev. Applied* **11**, 044094 (2019).
- [48] M. A. Cazalilla and J. B. Marston, Time-Dependent Sensitivity-Matrix Renormalization Group: A Systematic Method for the Study of Quantum Many-Body Out-of-Equilibrium Systems, *Phys. Rev. Lett.* **88**, 256403 (2002).
- [49] D. M. Kennes and V. Meden, Quench dynamics of correlated quantum dots, *Phys. Rev. B* **85**, 245101 (2012).
- [50] F. A. Wolf, I. P. McCulloch, and U. Schollwöck, Solving nonequilibrium dynamical mean-field theory using matrix product states, *Phys. Rev. B* **90**, 235131 (2014).
- [51] C. J. Lindner, F. B. Kugler, V. Meden, and H. Schoeller, Renormalization group transport theory for open quantum systems: Charge fluctuations in multilevel quantum dots in and out of equilibrium, *Phys. Rev. B* **99**, 205142 (2019).
- [52] A. Koga, Quantum Monte Carlo study of nonequilibrium transport through a quantum dot coupled to normal and superconducting leads, *Phys. Rev. B* **87**, 115409 (2013).
- [53] G. Cohen, E. Gull, D. R. Reichman, and A. J. Millis, Green's Functions from Real-Time Bold-Line Monte Carlo Calculations: Spectral Properties of the Nonequilibrium Anderson Impurity Model, *Phys. Rev. Lett.* **112**, 146802 (2014).
- [54] I. Krivenko, J. Kleinhenz, G. Cohen, and E. Gull, Dynamics of Kondo voltage splitting after a quantum quench, *Phys. Rev. B* **100**, 201104(R) (2019).
- [55] N. Dittmann, J. Splettstoesser, and N. Helbig, Nonadiabatic Dynamics in Single-Electron Tunneling Devices with Time-Dependent Density-Functional Theory, *Phys. Rev. Lett.* **120**, 157701 (2018).
- [56] N. Dittmann, N. Helbig, and D. M. Kennes, Dynamics of the Anderson impurity model: Benchmarking a nonadiabatic exchange-correlation potential in time-dependent density-functional theory, *Phys. Rev. B* **99**, 075417 (2019).
- [57] P. Wang and S. Kehrein, Flow equation calculation of transient and steady-state currents in the Anderson impurity model, *Phys. Rev. B* **82**, 125124 (2010).
- [58] S. Bock, A. Liliashvili, and T. Gasenzer, Buildup of the Kondo effect from real-time effective action for the Anderson impurity model, *Phys. Rev. B* **94**, 045108 (2016).
- [59] F. Randi, D. Fausti, and M. Eckstein, Bypassing the energy-time uncertainty in time-resolved photoemission, *Phys. Rev. B* **95**, 115132 (2017).
- [60] R. S. Souto, R. Avriller, A. L. Yeyati, and A. Martín-Rodero, Transient dynamics in interacting nanojunctions within self-consistent perturbation theory, *New J. Phys.* **20**, 083039 (2018).
- [61] I. Affleck, Boundary condition changing operations in conformal field theory and condensed matter physics, *Nucl. Phys. B Proc. Suppl.* **58**, 35 (1997).
- [62] R. Vasseur, K. Trinh, S. Haas, and H. Saleur, Crossover Physics in the Nonequilibrium Dynamics of Quenched Quantum Impurity Systems, *Phys. Rev. Lett.* **110**, 240601 (2013).
- [63] D. Bernard and B. Doyon, Conformal field theory out of equilibrium: a review, *J. Stat. Mech.: Theory Exp.* (2016) 064005.
- [64] C. Cohen-Tannoudji, B. Diu, and F. Laloe, *Quantum Mechanics*, Vol. I (Wiley-Interscience Publications, Paris, France, 1977).
- [65] M. Žonda, V. Pokorný, V. Janiš, and T. Novotný, Perturbation theory of a superconducting $0 - \pi$ impurity quantum phase transition, *Sci. Rep.* **5**, 8821 (2015).
- [66] H. T. M. Nghiem and T. A. Costi, Time-dependent numerical renormalization group method for multiple quenches: Application to general pulses and periodic driving, *Phys. Rev. B* **90**, 035129 (2014).
- [67] H. T. M. Nghiem and T. A. Costi, Generalization of the time-dependent numerical renormalization group method to finite temperatures and general pulses, *Phys. Rev. B* **89**, 075118 (2014).
- [68] We used the open-access Budapest Flexible DM-NRG code, <http://www.phy.bme.hu/~dmnrg/>; O. Legeza, C. P. Moca, A. I. Toth, I. Weymann, and G. Zarand, Manual for the Flexible DM-NRG code, [arXiv:0809.3143](https://arxiv.org/abs/0809.3143).
- [69] A. Weichselbaum and J. von Delft, Sum-Rule Conserving Spectral Functions from the Numerical Renormalization Group, *Phys. Rev. Lett.* **99**, 076402 (2007).
- [70] K. Wrześniewski and I. Weymann, Quench dynamics of spin in quantum dots coupled to spin-polarized leads, *Phys. Rev. B* **100**, 035404 (2019).
- [71] A. Weichselbaum, Tensor networks and the numerical renormalization group, *Phys. Rev. B* **86**, 245124 (2012).
- [72] J.-D. Pillet, P. Joyez, Rok Žitko, and M. F. Goffman, Tunneling spectroscopy of a single quantum dot coupled to a superconductor: From Kondo ridge to Andreev bound states, *Phys. Rev. B* **88**, 045101 (2013).
- [73] R. Žitko, J. S. Lim, R. López, and R. Aguado, Shiba states and zero-bias anomalies in the hybrid normal-superconductor Anderson model, *Phys. Rev. B* **91**, 045441 (2015).
- [74] J. Bauer, A. Oguri, and A. C. Hewson, Spectral properties of locally correlated electrons in a Bardeen-Cooper-Schrieffer superconductor, *J. Phys.: Condens. Matter* **19**, 486211 (2007).
- [75] T. Domański, I. Weymann, M. Barańska, and G. Górski, Constructive influence of the induced electron pairing on the Kondo state, *Sci. Rep.* **6**, 23336 (2016).
- [76] K. P. Wójcik and I. Weymann, Proximity effect on spin-dependent conductance and thermopower of correlated quantum dots, *Phys. Rev. B* **89**, 165303 (2014).
- [77] V. Meden, The Anderson-Josephson quantum dot—a theory perspective, *J. Phys.: Condens. Matter* **31**, 163001 (2019).
- [78] N. M. Gergs, C. B. M. Hørig, M. R. Wegewijs, and D. Schuricht, Charge fluctuations in nonlinear heat transport, *Phys. Rev. B* **91**, 201107(R) (2015).
- [79] J. Schulenburg, R. B. Saptsov, F. Haupt, J. Splettstoesser, and M. R. Wegewijs, Fermion-parity duality and energy relaxation in interacting open systems, *Phys. Rev. B* **93**, 081411(R) (2016).
- [80] J. Schulenburg, J. Splettstoesser, and M. R. Wegewijs, Duality for open fermion systems: Energy-dependent weak coupling and quantum master equations, *Phys. Rev. B* **98**, 235405 (2018).